Predicting Summer Arctic Sea Ice Concentration Intraseasonal Variability Using a Vector Autoregressive Model*

LEI WANG, XIAOJUN YUAN, MINGFANG TING, AND CUIHUA LI

Lamont-Doherty Earth Observatory, Columbia University, Palisades, New York

(Manuscript received 28 April 2015, in final form 19 November 2015)

ABSTRACT

Recent Arctic sea ice changes have important societal and economic impacts and may lead to adverse effects on the Arctic ecosystem, weather, and climate. Understanding the predictability of Arctic sea ice melting is thus an important task. A vector autoregressive (VAR) model is evaluated for predicting the summertime (May–September) daily Arctic sea ice concentration on the intraseasonal time scale, using only the daily sea ice data and without direct information of the atmosphere and ocean. The intraseasonal forecast skill of Arctic sea ice is assessed using the 1979–2012 satellite data. The cross-validated forecast skill of the VAR model is found to be superior to both the anomaly persistence and damped anomaly persistence at lead times of ~20–60 days, especially over northern Eurasian marginal seas and the Beaufort Sea. The daily forecast of ice concentration also leads to predictions of ice-free dates and September mean sea ice extent. In addition to capturing the general seasonal melt of sea ice, the model is also able to capture the interannual variability of the melting, from partial melt of the marginal sea ice in the beginning of the period to almost a complete melt in the later years. While the detailed mechanism leading to the high predictability of intraseasonal sea ice concentration needs to be further examined, the study reveals for the first time that Arctic sea ice can be predicted statistically with reasonable skill at the intraseasonal time scales given the small signal-to-noise ratio of daily data.

1. Introduction

Recent Arctic sea ice changes have important societal and economical impacts: the accelerated melting of Arctic sea ice in summer (e.g., Parkinson and Cavalieri 2008; Simmonds 2015) provides new fishery opportunities and increases the feasibility of trans-Arctic shipping (e.g., Eicken 2013), yet it may also lead to adverse effects on the Arctic ecosystem, weather, and climate (e.g., Serreze et al. 2007; Yang et al. 2015, submitted to *J. Climate*). Past studies have been mainly focused on the seasonal forecast of sea ice concentration (SIC) and sea ice extent (SIE), either using coupled dynamical models (e.g., Sigmond et al. 2013; Wang et al. 2013; Zhang et al. 2013; Chevallier et al. 2013; Merryfield et al. 2013; Peterson et al. 2015; Msadek et al. 2014) or statistical models based on past observations of the atmospheric and oceanic states [e.g., Lindsay et al. 2008; Kapsch et al. 2013; see Guemas et al. (2016) for more references]. Much less work has been done on the intraseasonal predictability of Arctic SIC, particularly for the summer melting season, which has the potential to impact the Arctic economy.

A vector autoregressive (VAR) model is evaluated for predicting summertime [May–September (MJJAS)] daily Arctic SICs in this study. This type of model has been used in previous studies to explore the interplay between atmospheric circulation and the Arctic sea ice intraseasonal variability. For example, Strong et al. (2009) analyzed the feedbacks between the North Atlantic Oscillation (NAO) and the Greenland sea ice dipole (GSD) in the winter using a VAR model. GSD has SIC anomalies of opposite signs in the Labrador and Barents Seas. They found that an NAO anomaly can induce a GSD anomaly in a week or so, while a GSD anomaly may lead to an NAO anomaly at a few weeks'

Denotes Open Access content.

* Lamont-Doherty Earth Observatory Contribution Number 7965.

Corresponding author address: Lei Wang, Lamont-Doherty Earth Observatory, Columbia University, 61 Rt. 9W, Palisades, NY 10964. E-mail: lwang@ldeo.columbia.edu

DOI: 10.1175/JCLI-D-15-0313.1

delay. Using a similar approach, Matthewman and Magnusdottir (2011) revealed positive feedbacks between the western Pacific pattern (a meridional dipole over the Bering Strait and the central Pacific in the midtropospheric geopotential height field; e.g., Wallace and Gutzler 1981) and the SIC in the Bering Sea during winter. These studies not only helped us to better understand the feedbacks between the atmospheric circulation and Arctic SIC but also showed the potential predictability of sea ice at the intraseasonal time scale. The usefulness of the VAR model has also been shown in other regions of the earth's climate system, for example, in predicting tropical Pacific and Atlantic sea surface temperature anomalies, as well as the Northern Hemisphere summer atmospheric low-frequency variability (e.g., Chapman et al. 2015; Lee et al. 2015; Wang et al. 2015). Similar statistical models, such as the Markov model (e.g., Chen and Yuan 2004), have been used extensively in the seasonal forecast of Antarctic and Arctic sea ice. The intraseasonal sea ice forecast is most beneficial in summer, when ice melting is at its maximum and human activities are practical in the Arctic. Therefore, in this study we focus on the daily sea ice prediction during the summer (May–September) season. The statistical modeling of Arctic sea ice has been mostly working with monthly or weekly data, but we will show in this study that there exists reasonable statistical forecast skill even in the much noisier daily SIC time series.

Although Arctic sea ice is considered to be largely affected by the atmospheric circulation (e.g., Fang and Wallace 1994; Deser et al. 2000; Serreze et al. 2003; Strong et al. 2009) on intraseasonal time scales, it has been found to impact the atmospheric circulation on time scales ranging from intraseasonal to decadal (e.g., Koenigk and Mikolajewicz 2009; Seierstad and Bader 2009; Matthewman and Magnusdottir 2011; Liu et al. 2012; Porter et al. 2012; Screen et al. 2013; Zhang et al. 2013; Henderson et al. 2014; Yang and Yuan 2014; Kim et al. 2014; Yang et al. 2015, manuscript submitted to *J. Climate*). Arctic sea ice is thus an essential component of the coupled atmosphere–ocean–sea ice system and its temporal evolution contains information from all components of the coupled system. As the first step, our attention in this study is focused on sea ice concentration alone to explore its predictability using the VAR model, in a similar way as in Kravtsov et al. (2009), Lee et al. (2015), and Chapman et al. (2015) for the sea surface temperature predictability.

The data and VAR model used in this study are described in the next section, as well as the metrics used to evaluate forecast skills. The predictions of Arctic sea ice are presented in section 3, followed by the summary and discussion of the main findings in section 4.

2. Data and method

The intraseasonal forecast skill of the Arctic SIC on a daily time scale is assessed using the 1979–2012 satellite data provided by the National Snow and Ice Data Center (NSIDC). SIC is the sea ice–covered area relative to the total at a given location in the ocean and thus ranges from 0 to 1 (or 0%–100%; corresponding to ice-free to fully ice-covered conditions). This SIC dataset has been generated using the bootstrap algorithm (Comiso 2000). The SIC data are available from 26 October 1978 every other day to 31 July 1987 and then daily afterward. The time series is linearly interpolated into the daily frequency between 1 January 1979 and 31 July 1987. The SIC is also resampled from the original 25 km × 25 km to the 225 km × 225 km grids to reduce the degrees of freedom (from 28 552 to 350) and computational costs. The reduction in spatial resolution does not affect the pan-Arctic-averaged SIC variability (mean square root of variance): 0.1608 for the original grid and 0.1621 for the coarser grid, and the regional differences in SIC variability are also not significant. Tests with the original and reduced resolutions produce very similar results, and hence we only show the results from the reduced resolution in this study. The empirical orthogonal function (EOF) analysis is used to further reduce the degrees of freedom of the summer (May–September) SIC data. The SIC is bounded within the range between 0 and 1, which often reaches the upper or lower bound and remains for an extended period. As a result, the deseasonalized or detrended SIC time series often contain artificial sharp changes around the time that SIC reaches the bounds. Sensitivity tests indicate that VAR models using deseasonalized or detrended SICs are dominated by the artificial sharp changes and are unable to represent well the physical variability in SICs. The climatological seasonal cycle and long-term trend of the SIC data are thus retained in the EOF decomposition, in order to avoid these artificial sharp changes in the SIC data due to summer melting. The leading (up to 100) principal components (PCs) are used to make the forecast using the VAR model, a further reduction in the degrees of freedom, and the predicted PCs are used to construct the SIC predictions. The climatological annual cycle is represented primarily by the first two PCs and the trend is visible in the first and the third PCs.

A general form of the Lth-order VAR can be written as follows:

$$\mathbf{x}_i = \sum_{j=N}^{L+N-1} \mathbf{A}_j \cdot \mathbf{x}_{i-j} + \mathbf{e}_i, \tag{1}$$

where $\mathbf{x}_i$ represents the variable $\mathbf{x}$ (i.e., leading PCs of SIC) at the ith time step and depends linearly on its

states at the previous N to $L + N - 1$ time steps with a forecast lead of N time steps. $\mathbf{A}_j$ is the coefficient matrix for the jth time step, and $\mathbf{e}$ represents the residual white noise process that is assumed to have no "memory." This model is a simplified and implicit form of the vector autoregressive moving average (VARMA) model (e.g., Love et al. 2008), which not only has the computational efficiency in estimating $\mathbf{A}$ using the least squares procedure but also retains some of the ability of the VARMA model in resolving long-range dependence in the time series. For example, the first-order ($L = 1$) VAR model used in this study,

$$\mathbf{x}_i = \mathbf{A}_N \cdot \mathbf{x}_{i-N} + \mathbf{e}_i, \tag{2}$$

is theoretically equivalent to a classic VARMA model with autoregressive order $N + 1$ and moving average order $N + 1$. This model further reduces to the Markov model used in previous studies (e.g., Chen and Yuan 2004) when $N = 1$. High-order VAR models sometimes are able to use more temporal information in predictors in order to gain extra forecast skill than the first-order VAR model at the cost of higher demand on the sample size of training data (e.g., Lütkepohl 2005). However, sensitivity tests indicate that high-order VAR models do not significantly improve the SIC forecast skill than the first-order VAR model (not shown). Therefore, in this study we show results of the first-order VAR model with different EOF truncations (the number of leading PCs to keep); for example, VAR E12 represents the first-order VAR model with the first 12 PCs of SIC as both the predictors and predictands.

The VAR model is used to forecast daily SIC with a lead time N up to 80 days and for the extended summer season (May–September). The use of this extended period is necessary to meet the degree-of-freedom requirements of the VAR model. The number of samples generally needs to be at least one order larger than the number of predictors to ensure the robustness and accuracy of the estimation of the coefficient matrix $\mathbf{A}$ (e.g., Johnstone 2001). The forecast is made retrospectively; that is, the coefficient matrix $\mathbf{A}$ in Eq. (2) used to predict the SICs of a given summer is estimated by the SICs of all the other 33 summers. Variable $\mathbf{A}_N$ is estimated using all the pairs of days that are separated by N days. For a lead time of 80 days (i.e., $N = 80$), the number of available sample pairs is the total number of days in each summer (153 for May–September) minus N—that is, $153 - 80 = 73$—multiplied by the number of training summers (33 out of 34 summers of 1979–2012), which is $73 \times 33 = 2409$. Moreover, the extended summer also ensures that the key period of the sea ice melting processes—that is, August and September—is always included for the model evaluation for all lead times. For example, the period from 20 July to 30 September is predicted using initial conditions from 1 May to 9 July, for $N = 80$. In contrast, only the last 12 days of September could be predicted for $N = 80$ if only 3 months (July–September) were included.

The forecast skill of the VAR model is evaluated by 1) temporal anomaly correlation (i.e., anomaly autocorrelation), 2) root-mean-square error (RMSE), 3) mean ice-free date error, and 4) September mean sea ice extent error. For each lead time N, the SIC is reconstructed from the predicted PCs for all starting days to form a single continuous time series (e.g., lumping together from 20 July to 30 September of all years between 1979 and 2012 for $N = 80$) to be evaluated with observations. The predicted SIC is brought back to its physical bound 0 or 1 if exceeding the range of (0, 1). The anomaly correlation and RMSE are calculated in the standard way, that is, between the time series of observed and predicted SIC anomalies at each location (note that the climatological mean annual cycle is removed to obtain the SIC anomalies for all skill evaluations). The spatially averaged anomaly correlation is computed via the Fisher's z transformation [see Wilks (1995) for details], so that the resulted correlation coefficient is Gaussian distributed and thus directly additive. The ice-free date is defined as the day during the melting season when SIC drops to and remains below 0.15 or 15% (Stammerjohn et al. 2008, 2012). The grid points where SIC never drops below 0.15 by the end of September are assigned an ice-free date of 1 October. The SIE is calculated as the number of grid points at which SIC is at least 0.15 multiplied by the area of each grid box, 225 km $\times$ 225 km. The VAR model tends to overestimate the September SIE, similar to other statistical models (e.g., Yuan et al. 2015, manuscript submitted to *J. Climate*), and thus a bias-correction procedure is used to reduce the forecast error in the September SIE. This procedure linearly fits the daily SIE anomalies (SIE_a) to the future SIE errors or biases (SIE_b) at the lead time N, similar to the autoregressive model:

$$\mathrm{SIE}_b(t, N) = \alpha_N[\mathrm{SIE}_a(t - N)] + \beta, \tag{3}$$

where the slope of the regression α represents the linear dependence on SIE_a and the intercept β is the constant bias at zero anomaly. This bias-correction method is constructed such that no information beyond the lead time is required and is thus a forecast method for the SIE residual that has not been resolved by the predicted SICs. The daily (uncorrected and corrected) SIEs are averaged over September of each year to obtain the September mean SIEs.

3. Results

The summer Arctic SIC shows pronounced daily variability over marginal seas, especially in the Beaufort,

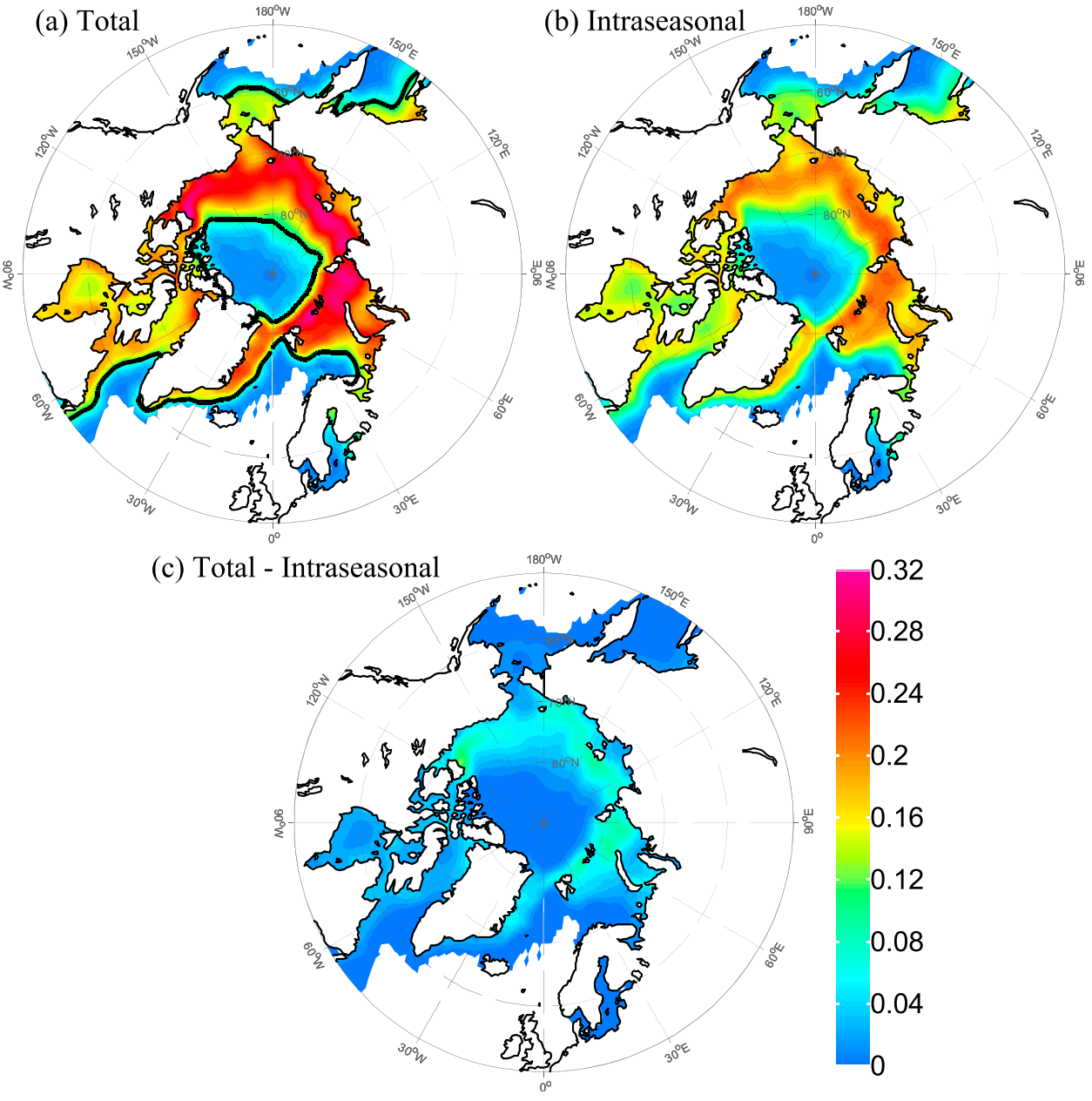

FIG. 1. (a) Total, (b) intraseasonal, and (c) total minus intraseasonal daily variability of Arctic SIC of May–September 1979–2012 in standard deviations. The black contours in (a) indicate variability equal to 0.1.

East Siberian, Laptev, Kara, and Barents Seas (Fig. 1a). At each grid point, the climatological mean seasonal cycle (the daily climatology of 34-yr SIC) is removed from the total SIC and the standard deviation of the remaining anomaly—that is, the total daily variability of SIC—is shown in Fig. 1a. The seasonal mean of each summer can be further removed from the SIC anomaly, which effectively removes the interannual variability. The standard deviation of the residual time series represents the intraseasonal component of the total SIC daily variability, as shown in Fig. 1b. The difference between the total and the intraseasonal components gives the interannual to decadal SIC variability (Fig. 1c). The total summer SIC variability is dominated by the intraseasonal component, while the interannual and decadal components explain only up to one-quarter of the total (Figs. 1b,c vs 1a). The regions with total daily variability less than 0.1 (separated by black contours in Fig. 1a) mainly consist of a permanently ice-covered area around the North Pole with SICs close to 1 throughout the year,

TABLE 1. The 60-day lead forecast skill of the September monthly mean SIE in terms of the anomaly correlation coefficient r and RMSE. The subscript c indicates bias correction and the subscript d indicates detrending.

	Models						
	E12	E17	E21	E25	E29	E32	E47
Cumulative variance captured	46%	54%	58%	62%	65%	68%	76%
r	0.88	0.87	0.85	0.86	0.87	0.87	0.85
r_c	0.88	0.87	0.85	0.86	0.87	0.87	0.85
RMSE ($\times 10^6$ km^2)	1.22	1.22	1.25	1.26	1.26	1.26	1.31
RMSE$_c$ ($\times 10^6$ km^2)	0.52	0.54	0.57	0.55	0.54	0.54	0.56
r_d	0.63	0.59	0.53	0.60	0.60	0.61	0.55
r_{dc}	0.63	0.59	0.53	0.60	0.60	0.61	0.55
RMSE$_d$ ($\times 10^6$ km^2)	0.59	0.63	0.66	0.67	0.65	0.65	0.66
RMSE$_{dc}$ ($\times 10^6$ km^2)	0.58	0.59	0.62	0.58	0.57	0.57	0.59

and the southern edge of the marginal seas, where sea ice melts quickly in early summer and does not reemerge until the next freezing season. The predictability of SIC in these regions is thus intrinsically very high due to the small variability. Therefore, in this study we focus on the regions with total daily variability greater than 0.1 and refer to these regions as ''pan-Arctic'' (the warm color–shaded regions between the black contours in Fig. 1a). These regions also cover the crucial part for the trans-Arctic transportation routes (e.g., Serreze et al. 2007).

a. Predicting sea ice concentration

The VAR model is first run with various EOF truncations (1–50 modes, largely reduced from the 350 physical grid points) with lead times of 1–80 days. Samples of optimal configurations in EOF truncations (12, 17, 21, 25, 29, 32, and 47 modes) are chosen to illustrate the forecast skill of the VAR model. The cumulative variance captured by these EOF truncations varies from 46% to 76%, as listed in Table 1, excluding the first two EOF modes representing the seasonal cycle. In Fig. 2, we show the temporal anomaly correlations and the root-mean-square errors as a function of lead time and averaged over the pan-Arctic region. The cross-validated pan-Arctic mean forecast skill of the VAR model as measured by anomaly correlation is superior to those of anomaly persistence and damped anomaly persistence for lead times longer than 20 days (Fig. 2a). The persistence of anomaly at the starting date superimposed on top of the daily climatology is a good indicator of natural predictability in sea ice and can be used as a reference for evaluating the model skill (gray solid curve in Fig. 2a). The damped anomaly persistence (gray dashed curve in Fig. 2a; note that the anomaly persistence and the damped anomaly persistence curves are almost perfectly on top of each other) is another useful reference for forecast skill, where the amplitude of the anomaly is assumed to reduce in time exponentially at a time scale of the local autocorrelation time (e.g., Griffies and Bryan 1997). In the limit of long lead time, the amplitude of the anomaly is damped toward zero, and therefore the damped anomaly persistence approaches the climatological mean asymptotically. Note that both the anomaly persistence and the damped anomaly persistence predictions are corrected as is done for the predicted SICs, if exceeding the physical range of 0–1. The anomaly correlation is higher with more EOF modes retained at a lead time shorter than 3 weeks, whereas at a longer lead time, retaining fewer EOFs makes the better forecast (color curves in Fig. 2a). The correlation coefficients are calculated using daily time series of 34 summers (each summer has 153 days from May to September). The degrees of freedom range from 5166 ($= 152 \times 34 - 2$) for a 1-day lead to 2480 ($= 73 \times 34 - 2$) for an 80-day lead. The anomaly correlations of the VAR model are thus statistically significant at the 99% level for all lead times because of the large degrees of freedom. The RMSEs show similar behavior as the anomaly correlation in that the VAR model has smaller RMSEs than the anomaly persistence at a lead time starting from approximately 15 days (Fig. 2b). Although the overall forecast skills are not very sensitive to the number of EOF modes retained in the VAR model, the pan-Arctic skills are slightly higher when 25 modes were included (green dashed curves in Fig. 2). Despite this small sensitivity of the pan-Arctic mean skill, regional skills are much more sensitive to the EOF truncations for long lead times as it will show in the example of the Kara Sea below. On the other hand, retaining more modes only improves forecast skills for short lead times ($<$15 days or so) and degrades skills for longer lead times. For example, the VAR model with 100 EOFs shows better skill (is much closer to the anomaly persistence) than the other lower EOF truncations in the first week or so (dark red curves in Fig. 2).

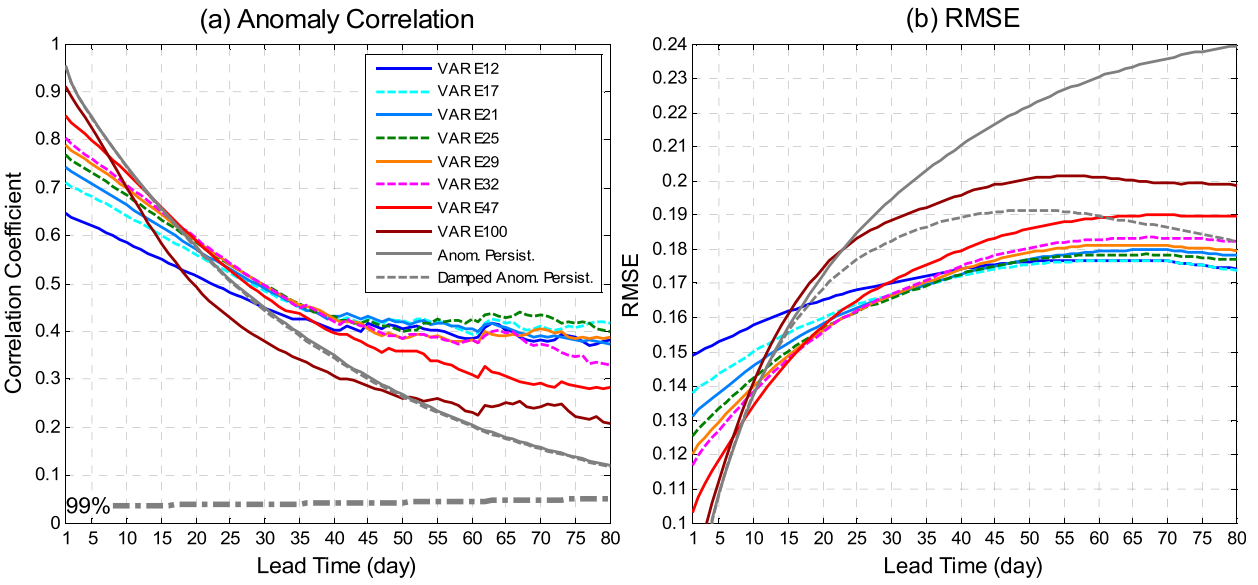

FIG. 2. (a) Temporal anomaly correlation coefficient and (b) RMSE averaged over regions with MJJAS SIC variability greater than 0.1 for a lead time ~1–80 days for the VAR model with a sample of a number of EOFs. The anomaly persistence in the observations is plotted in solid gray and the damped anomaly persistence in dashed gray. The dashed–dotted gray curve in (a) represents the statistical significance of the correlation coefficient at the 99% level by the Student's *t* test.

For lead times longer than 20 days, the VAR model shows better forecast skill than the anomaly persistence in most of the Arctic region, especially over marginal seas, such as the Chukchi Sea, Kara Sea, and Baffin Bay (e.g., Figs. 3a–c for a 40-day lead). At these marginal seas, the model skills measured by correlations increase by 0.1–0.2 (Fig. 3c), and the RMSE reduces by 0.08–0.1 for the VAR model over the damped anomaly persistence at the 40-day lead (Figs. 3d–f). The most pronounced improvements occur in the Kara and Barents Seas (Figs. 3c,f). The SICs of the Kara and Barents Seas have been shown to have pronounced sea ice variability and strong climate impacts (e.g., Smedsrud et al. 2013; Scaife et al. 2014; Yang et al. 2015, manuscript submitted to *J. Climate*). These two marginal seas are thus chosen as examples of assessing regional sea ice forecast skills. The gridded SICs within each region were spatially averaged to form the SIC time series for evaluation. In the Barents Sea, the VAR model shows better forecast skill than the anomaly persistence at lead times of 20–60 days (Fig. 4a). Although the improvements in anomaly correlation were small, the RMSE is reasonably reduced (Fig. 4b). In contrast, the forecast skill improvements over the anomaly persistence in the Kara Sea are mainly for the anomaly correlation than for the RMSE (Figs. 4c,d). It is also worth noting that there exists a clear monotonic dependence of the forecast skill on the number of EOFs included in the VAR model for the Kara Sea, but the relationship is much less clear in the Barents Sea, indicating somewhat different physical processes controlling the sea ice variability in the two regions. It also suggests that the sea ice in the Barents Sea is more variable than that in the Kara Sea.

The domain-averaged SIC anomaly time series at the Barents and Kara Seas are compared to help understand the physical differences in their predictability. The two time series (not shown) have very similar ranges of interannual variability, both around 0.04, whereas the Barents Sea has larger amplitude of intraseasonal variability in SIC (0.11) than that for the Kara Sea (0.09). A likely explanation is that the Barents Sea is directly exposed to the warm and salty Norwegian Current, a poleward extension of the North Atlantic Current, and thus it has much stronger air–ocean–ice exchanges due to its significantly lower mean SIC than the Kara Sea. In the Barents Sea, the heat exchange between the atmosphere and ocean is more active than in the Kara Sea (e.g., Smedsrud et al. 2013).

b. Predicting the ice-free date

To illustrate sea ice melting behaviors through the season, we plot domain-averaged SIC time series in the Barents and Kara Seas as examples (Fig. 5). May SIC usually starts close to 1 in the Kara Sea, while in the Barents Sea we see much higher variability in the average SIC on 1 May, especially in the twenty-first century being typically below the climatological mean (Fig. 5a). This is consistent with the extra heating

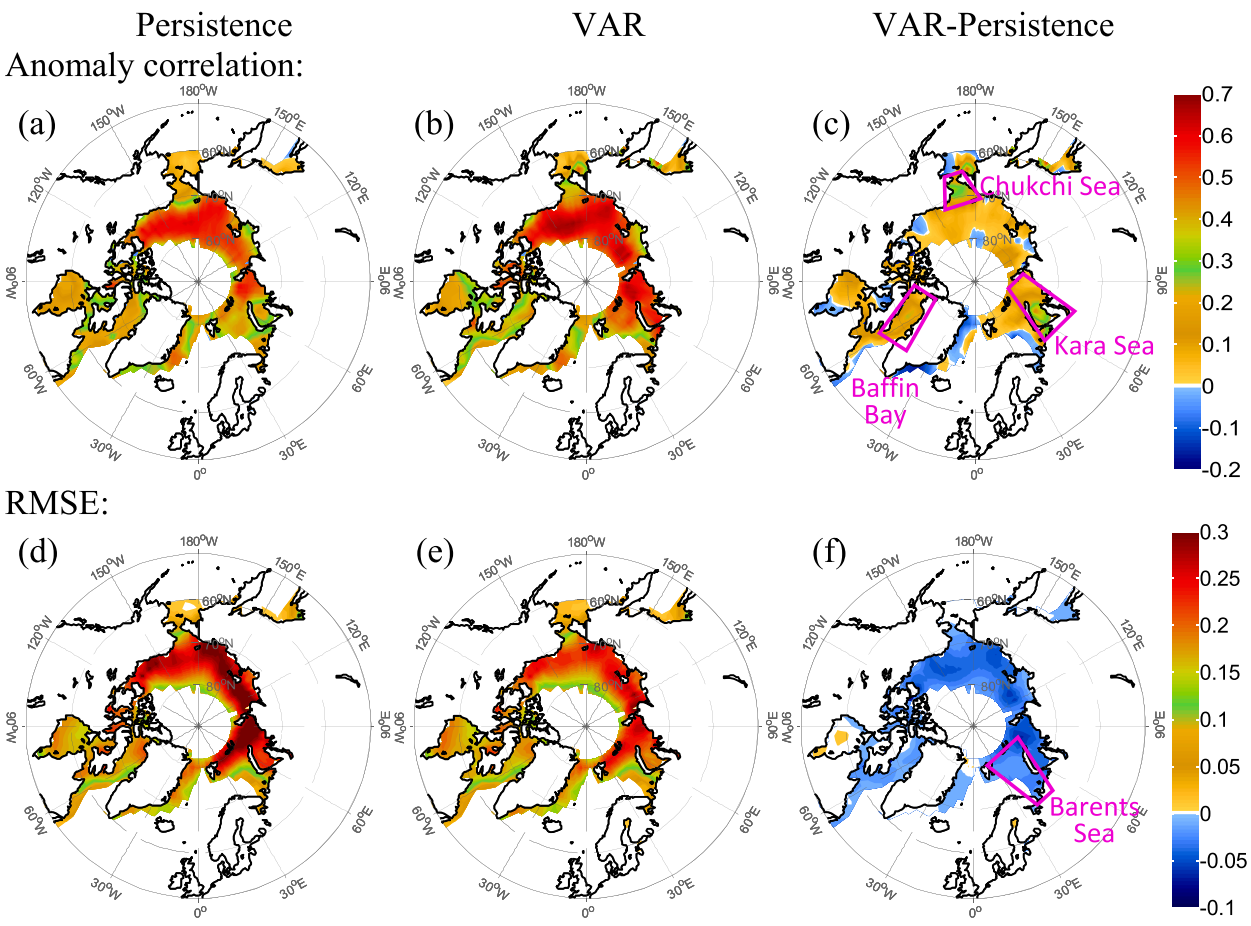

FIG. 3. The 40-day lead anomaly correlation of (a) the observed damped anomaly persistence, (b) the VAR E25 model, and (c) their difference. (d)–(f) As in (a)–(c), but for the RMSE.

imported by the warmer and stronger North Atlantic Current in recent years (e.g., Polyakov et al. 2012). By September, the Barents Sea is close to ice free (SIC < 0.15). In the Kara Sea, on the other hand, the initial sea ice cover in early May remains rather constant throughout the study period, and the melting of the sea ice occurs earlier (Fig. 5b, dashed curves compared with solid curves) in recent years. September ice minimum exhibits large variability in the Kara Sea, although it is close to open water in recent years. Understanding the melting processes and the ability of predicting SIC through the season would lead to a prediction of ice-free dates.

The ice-free date is defined as the date at each grid point where SIC drops to and stays below 0.15 (15%) (e.g., Stammerjohn et al. 2008, 2012). For example, in Fig. 5 the ice-free dates can be estimated as the intersections between the SIC (colored curves) and the 0.15 (15%) threshold (black line). Note that this example is just illustrative, as Fig. 5 shows that the spatially averaged SIC and the ice-free date estimated here are not equal to the spatially averaged ice-free date of this region. The melting of the Arctic sea ice is a rapid process, which often occurs within a few days to a few weeks at most locations and is thus not well resolved in the monthly SIC data. The forecast of the daily SICs made by the VAR model, however, allows predictions of the ice-free date. In addition, the ice-free date varies greatly from year to year (e.g., Fig. 5), which makes it challenging to predict. At each location and each summer, the ice-free date is identified from both the observed SIC and the predicted SIC time series at each lead time based on the 0.15 threshold. The absolute error (i.e., the absolute value of the error) in the ice-free date averaged over all years, or the mean absolute error, is a measure of how accurately the ice-free date is predicted, regardless of being early or late. The mean absolute error averaged over the pan-Arctic region increases with lead time for the anomaly persistence (solid gray curve in Fig. 6a), the damped anomaly persistence (dashed gray

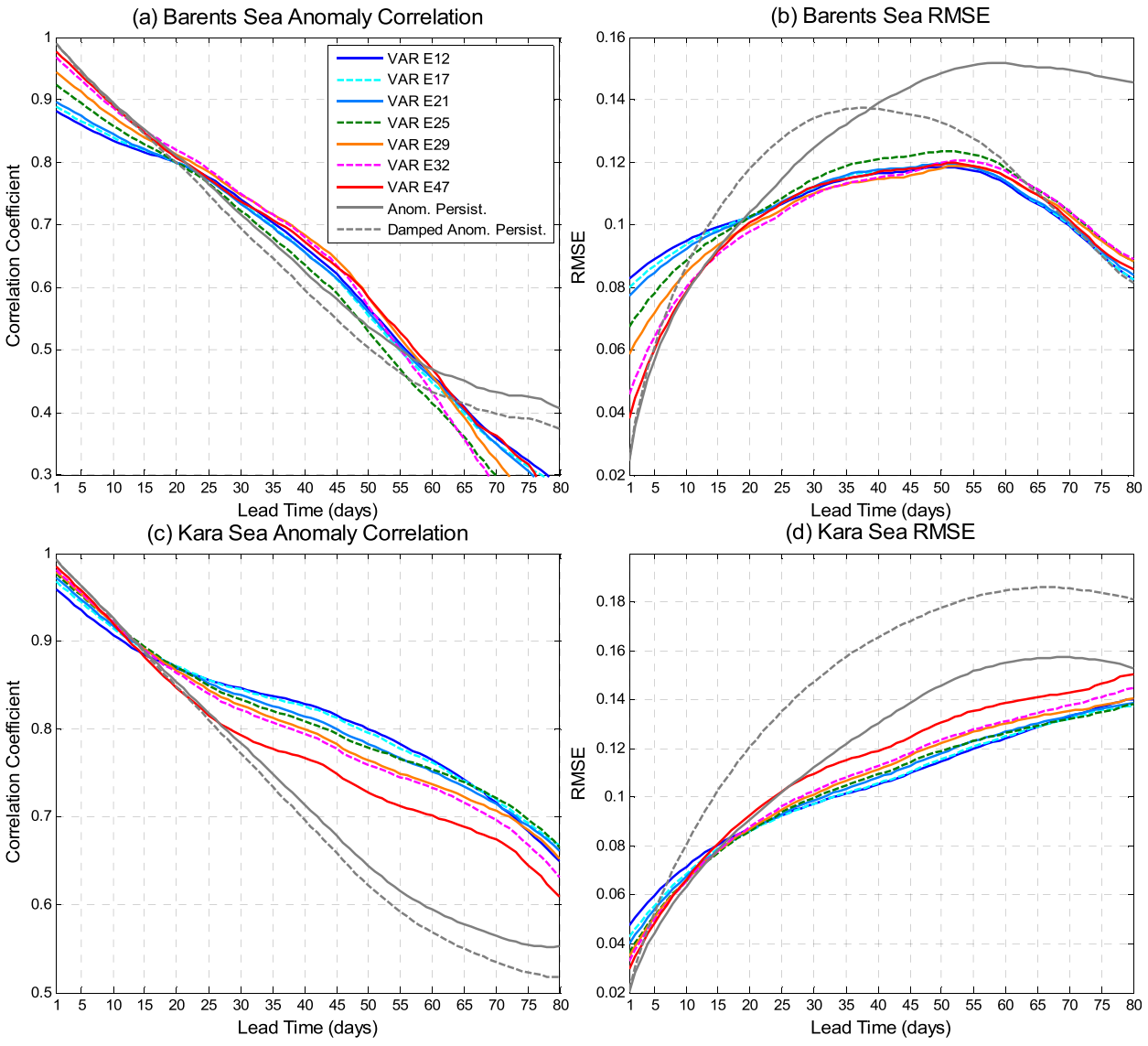

FIG. 4. Cross-validated model skills measured by (a) anomaly correlation and (b) RMSE between model predictions and observations of summer (MJJAS) for Barents Sea SIC as a function of lead times. (c),(d) As in (a),(b), but for the Kara Sea.

curve in Fig. 6a), and the forecasts (blue curve in Fig. 6a). The VAR model forecasts show a reduction in mean absolute error compared to the anomaly persistence for lead times longer than 25 days and the largest improvements (up to 7 days) occur at around the ~50–60-day lead (blue vs solid gray in Fig. 6a). The VAR model, however, is only slightly superior to the damped anomaly persistence for lead times of 25–60 days (blue vs dashed gray in Fig. 6a). To remove any possible systematic bias in the VAR model forecasts, a constant bias correction is applied to the ice-free date predictions. For each year and each grid point, the average bias of all the other 33 years' dates is subtracted from this year's predicted date (i.e., similar to the take-one-year-out cross validation). The bias-corrected ice-free dates show an improvement of about 7 days on average for lead times of 25–60 days (red vs blue in Fig. 6a). On the other hand, a positive (negative) mean error measures how late (early) on average the ice-free date is predicted. A small mean absolute error means accurate prediction of the ice-free date in most years, while a small mean error indicates the averaged timing is captured by the forecast although it might be too early in some years and too late in other years. The anomaly persistence systematically produces a later ice-free date for lead times greater than 10 days and the positive error increases with the lead time (solid gray curve in Fig. 6b), whereas the mean error of the damped anomaly persistence remains at

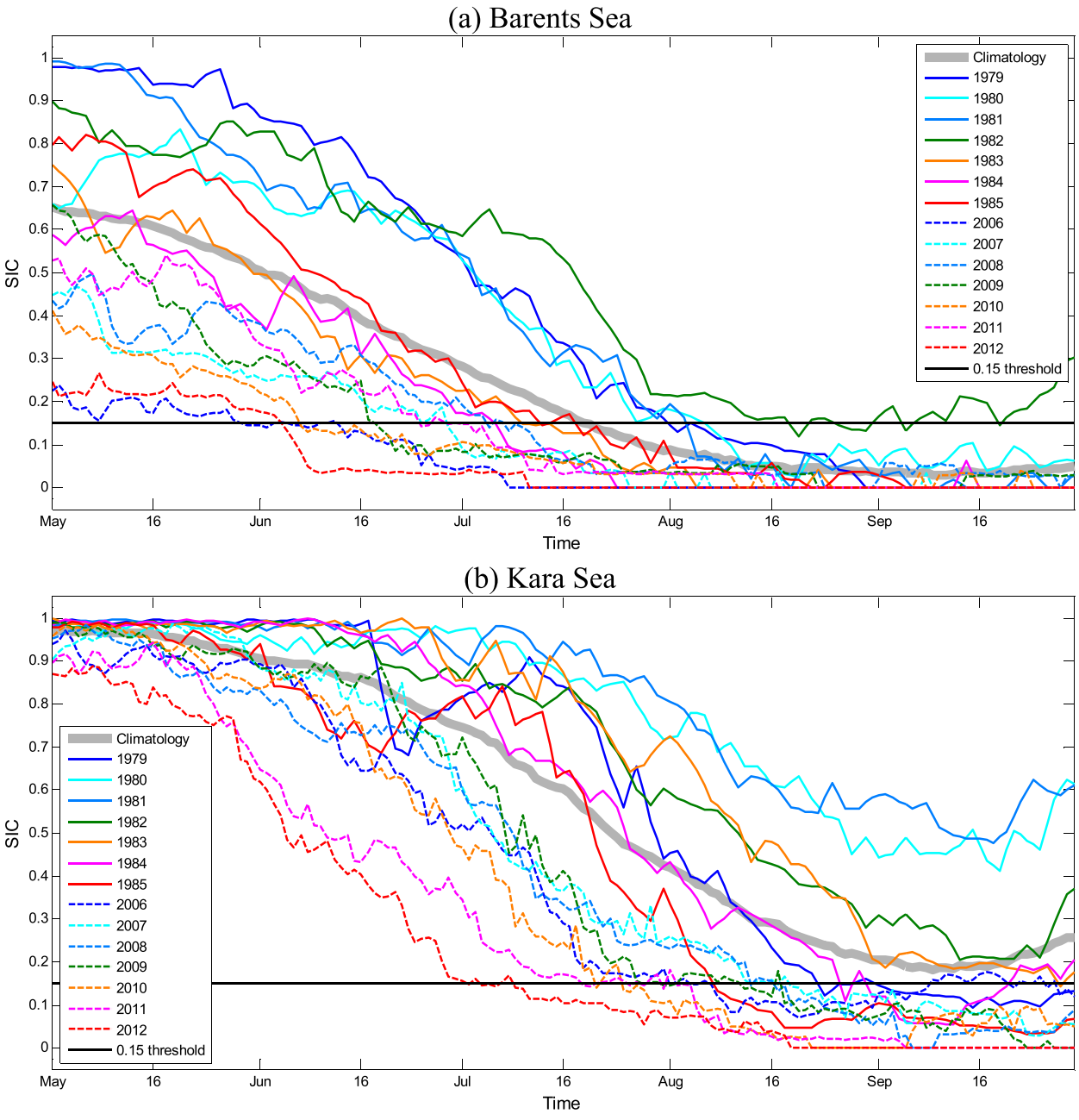

FIG. 5. The time series of regionally averaged SIC at the (a) Barents Sea and (b) Kara Sea. Solid curves represent years from 1979 to 1985, while dashed curves represent years from 2006 to 2012.

around 5–7 days later for lead times of ~10–60 days and turns to early melt at longer leads (dashed gray curve in Fig. 6b). The VAR model shows an advantage of 2 days or so compared with the damped anomaly persistence for lead times of ~25–60 days (blue vs dashed gray in Fig. 6b). The bias-corrected VAR model ice-free date shows near-zero mean error (red curve in Fig. 6b), since the mean bias is removed. The number of modes included in the VAR model does not seem to significantly influence the mean absolute error and the mean error for lead times longer than 30 days (not shown), implying that the melting processes in the Arctic are likely to be controlled primarily by several leading modes.

The errors in the ice-free date also vary significantly in space. The 60-day lead mean absolute error by the anomaly persistence is greatest in the marginal seas, for example, up to 40 days at the Bering Sea, Chukchi Sea, Kara Sea, Baffin Bay, and Hudson Bay (red regions in

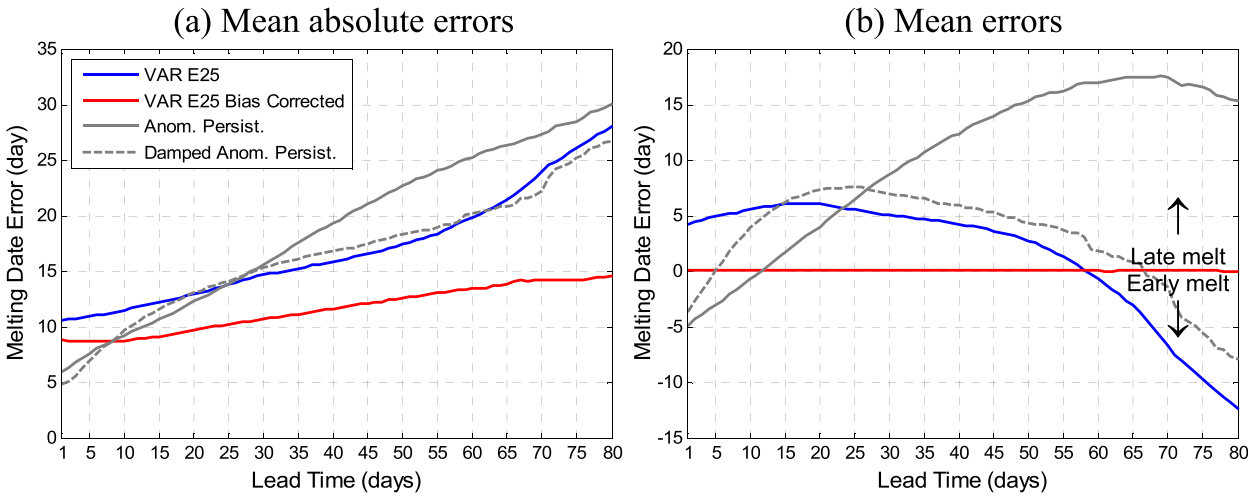

FIG. 6. The pan-Arctic-averaged (a) mean absolute errors and (b) mean errors in the ice-free date as a function of lead times.

Fig. 7a). The damped anomaly persistence largely reduces the mean absolute error in most of the above-mentioned regions except for the Chukchi Sea (Fig. 7b). The VAR E25 model further reduces it to about 10–20 days over the same region (Fig. 7c). On the other hand, the mean error represents the systematic bias in the timing of the melting. The mean error by the anomaly persistence is in general fairly close to the mean absolute error (cf. Figs. 7a,d), implying the anomaly persistence overestimates the ice-free date (late melt) in most years. In contrast, the damped anomaly persistence and the VAR model with bias correction have less mean errors than mean absolute errors (Figs. 7b,c vs 7e,f) and hence have much weaker systematic biases than the anomaly persistence. On average, the VAR model with bias correction tends to predict the ice-free date too late in the northern Barents Sea, the Kara Sea, the western Beaufort Sea, and the Bering Sea, as well as in part of the Greenland Sea, while it predicts the melt date too early in the Hudson Bay, the Laptev Sea, and the southern Barents Sea (Fig. 7f).

The melting processes in the Barents and Kara Seas are intricate and their ice-free dates vary significantly from year to year as shown in Figs. 5 and 8. In the Barents Sea, there is a linear dependence of ice-free dates on early May (first 10 days of May) mean SIC: higher SICs in early May result in later ice-free dates (Fig. 8). It is likely due to its direct exposure to the Norwegian Current, since atmospheric circulation seems not to directly influence the secular trend in the summer Arctic sea ice (e.g., Deser and Teng 2008). In the Kara Sea, however, this linear relationship only exists in recent years, as its early May SIC is very close to 1 (100%) in most years. This indicates that the melting processes in the Kara Sea have become more influenced by ocean currents and more coupled to atmospheric variability recently.

To illustrate the VAR model's forecast skills in capturing the large interannual variability of sea ice melting processes in these two regions, we present the scatterplots of observed and predicted ice-free dates spatially averaged in each region in Fig. 9. The damped anomaly persistence is very close to the climatological mean at the 60-day lead time and is thus not included in this comparison. The VAR predictions (circles in Fig. 9) are generally closer to the diagonal line (representing perfect predictions) than the anomaly persistence (squares in Fig. 9), although both methods tend to overestimate the ice-free dates (predict late melt) in the Kara Sea for recent years (hollow symbols in Fig. 9b). The improvements over the anomaly persistence are more pronounced for the Kara Sea (Fig. 9b) than those for the Barents Sea (Fig. 9a), consistent with the corresponding improvements in the anomaly correlation of regional mean SIC (Figs. 4a,c). The ice-free date errors for the Barents Sea are not very sensitive to the initial (early May) SICs for both anomaly persistence and VAR model forecasts. In contrast, the ice-free date errors for the Kara Sea are much larger for the years with lower initial SICs (the third numbers in Fig. 9b for VAR model predictions and anomaly persistence predictions, respectively), although the interannual variations in the initial SIC are much smaller in the Kara Sea than those of Barents Sea (Fig. 8). The contrast in the ice-free date errors between these two regions implies that the earlier ice-free dates of the Kara Sea in recent years are induced by external factors, such as ocean currents, atmospheric heat transport, and coupling to the atmospheric bridge

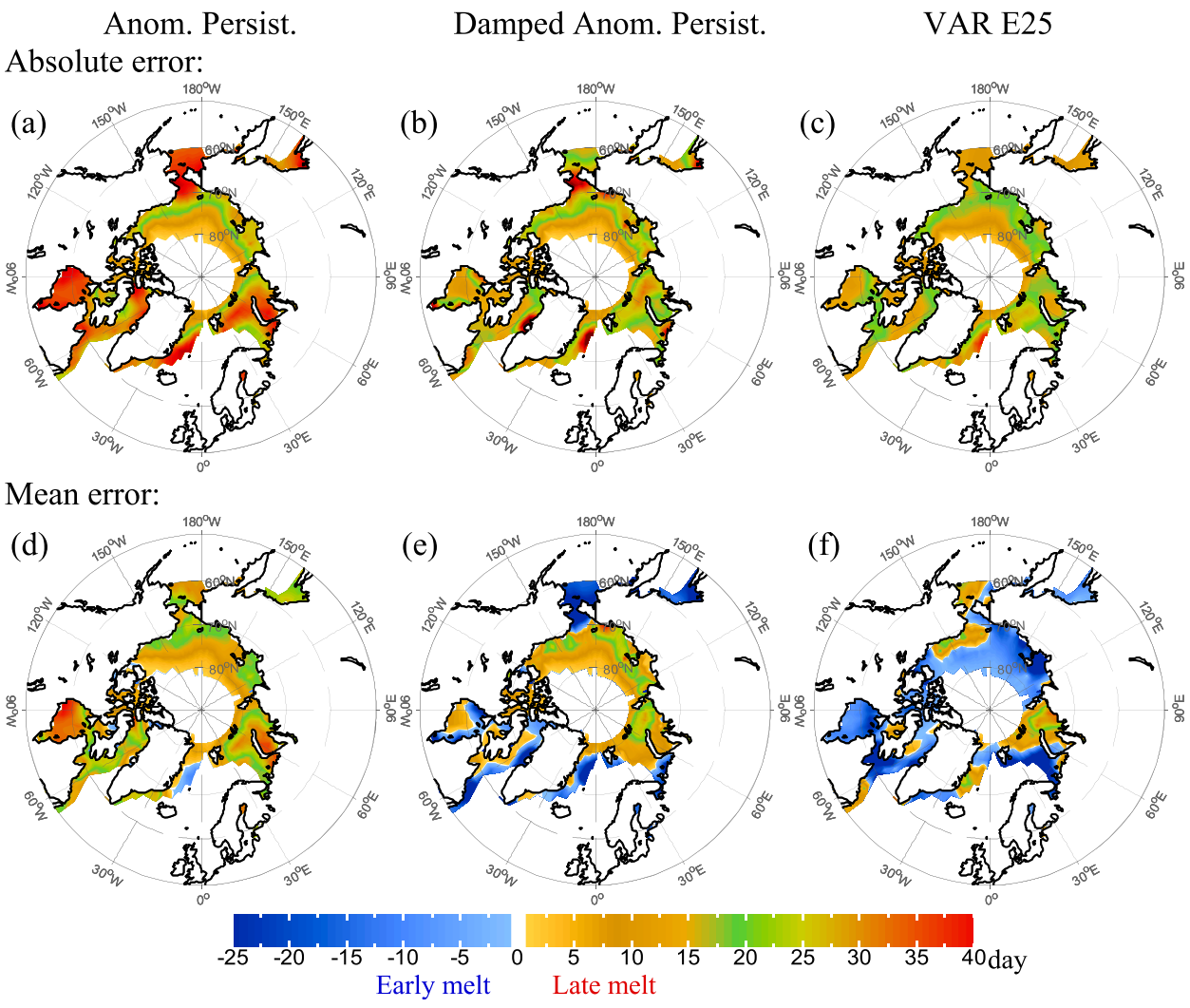

FIG. 7. The 60-day lead absolute errors in the ice-free date of (a) the observed anomaly persistence, (b) the observed damped anomaly persistence, and (c) the VAR E25 model with the constant bias correction. (d)–(f) As in (a)–(c), but for the mean errors.

(e.g., Liu and Alexander 2007), which is not fully resolved by the statistical methods that use mainly past sea ice information to build the prediction operators [such as **A** in Eq. (2)] and might be better captured with extra information from the atmosphere and ocean.

c. *Predicting sea ice extent*

The Arctic sea ice extent has a distinct annual cycle with minimum extent in September. The September SIE minimum is a widely used index in evaluating the forecast models in the Arctic sea ice community (e.g., Stroeve et al. 2014) and in quantifying polar amplification (e.g., Holland and Bitz 2003). The VAR model tends to overestimate the September total SIE, for example, at a mean bias of around 1.2×10^6 km^2 for 60-day lead forecasts. The bias is weakly negatively correlated with the magnitude of the SIE anomaly (Fig. 10a), which allows us to conduct a bias correction based on the linear regression of initial SIE anomaly [see Eq. (2)] similar to that by Yuan et al. (2015, manuscript submitted to *J. Climate*). The bias correction is applied to the daily SIE forecasts and the corrected September daily SIE is then averaged to obtain the September monthly mean SIE. This bias correction does not make notable changes on the anomaly correlation but can significantly improve the RMSE. For example, the September monthly mean SIE predicted by the VAR E12 model at the 60-day lead (blue curve in Fig. 10b) has a bias that is about 0.5×10^6 km^2 in the 1980s and increases to almost 2×10^6 km^2 in recent years. The correction removes not only the mean bias but also the errors in the trend (red curve in Fig. 10b). The RMSE is reduced by more than half at all lead times (Fig. 10c). On

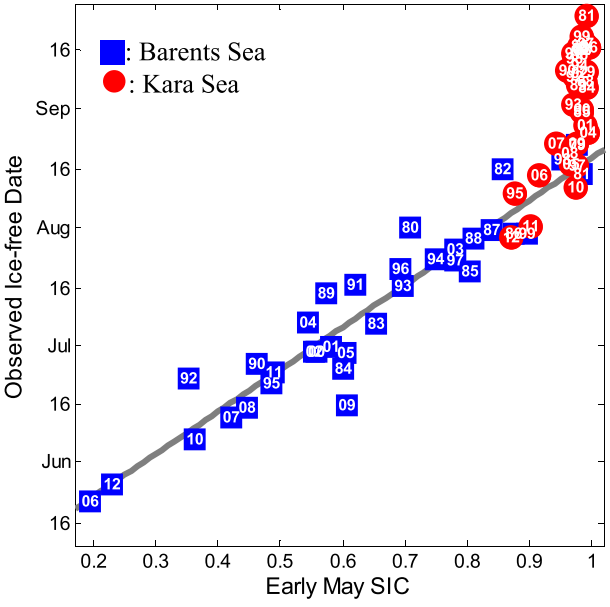

FIG. 8. The scatterplots of observed ice-free dates and early May (1–10 May mean) SICs regionally averaged at the Barents Sea (squares) and the Kara Sea (circles) labeled with the last two digits of corresponding years. The gray line is the linear fit of Barents Sea data.

the other hand, the anomaly correlation remains at 0.88 for the original and bias-corrected September mean SIE at the 60-day lead. As it can be seen in Fig. 10b, a major part of the bias comes from the rapid decline trend in recent decades and therefore we also calculated the anomaly correlation coefficients and RMESs using the de-trended SIE time series (i.e., the secular trend in SIE of each day is removed). Once again the anomaly correlation remains unchanged for the bias correction (r_d vs r_{dc} in Table 1). Without the bias correction, the RMSEs for the detrended SIE time series are much smaller than those for the original (RMSE vs RMSE$_d$ in Table 1). The bias correction only slightly reduces the RMSE for the detrended time series (RMSE$_d$ vs RMSE$_{dc}$ in Table 1), confirming that the SIE bias primarily consists of the trend component, consistent with the abovementioned findings in Fig. 10b.

This linear regression–based bias-correction method is similar to the methods developed by Kharin et al. (2012) and Fučkar et al. (2014) with a few minor differences. Kharin et al. (2012) express the trend explicitly as a linear time-dependent term in the bias correction, whereas Fučkar et al. (2014) replace the trend term by initial conditions in observations that are temporally smoothed to avoid impacts from synoptic fluctuations. Since the total Arctic SIE used in our study is not very sensitive to synoptic fluctuations, the performance of our method [i.e., Eq. (2)] is almost identical to that of Fučkar et al. (2014) and is slightly better than that of Kharin et al. (2012) (not shown).

4. Conclusions and discussion

A data-driven statistical model, the VAR model, has been evaluated for predicting the summertime (May–September) daily Arctic sea ice concentration. This VAR model is found to be able to well predict the Arctic

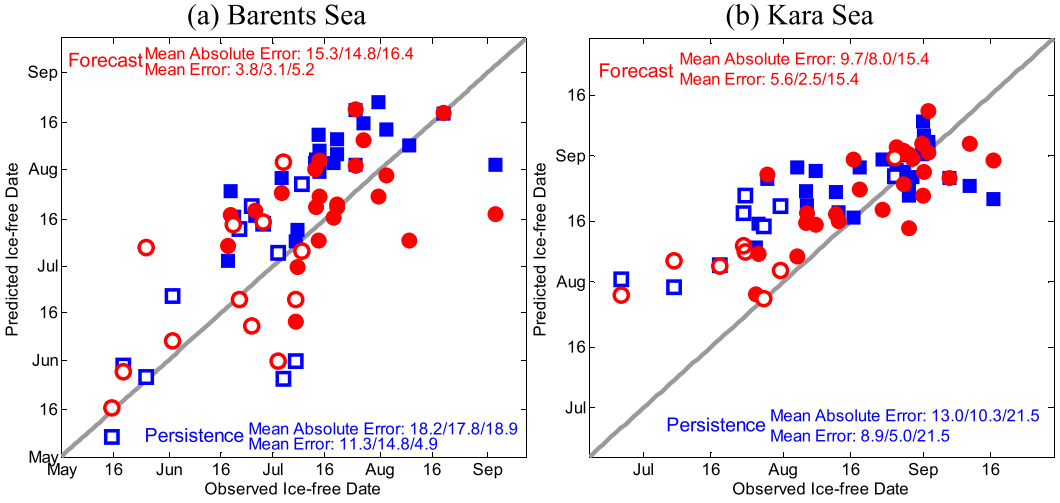

FIG. 9. The scatterplots of predicted (at the 60-day lead time and bias corrected) and observed ice-free dates regionally averaged at the (a) Barents Sea and (b) Kara Sea. The predictions based on anomaly persistence are plotted in square symbols, and those based on the VAR model are in circle symbols. The years with initial (1–10 May mean) SIC above (below) average are plotted in filled (hollow) symbols. The errors are listed in the order of all years, high initial SIC years, and low initial SIC years.

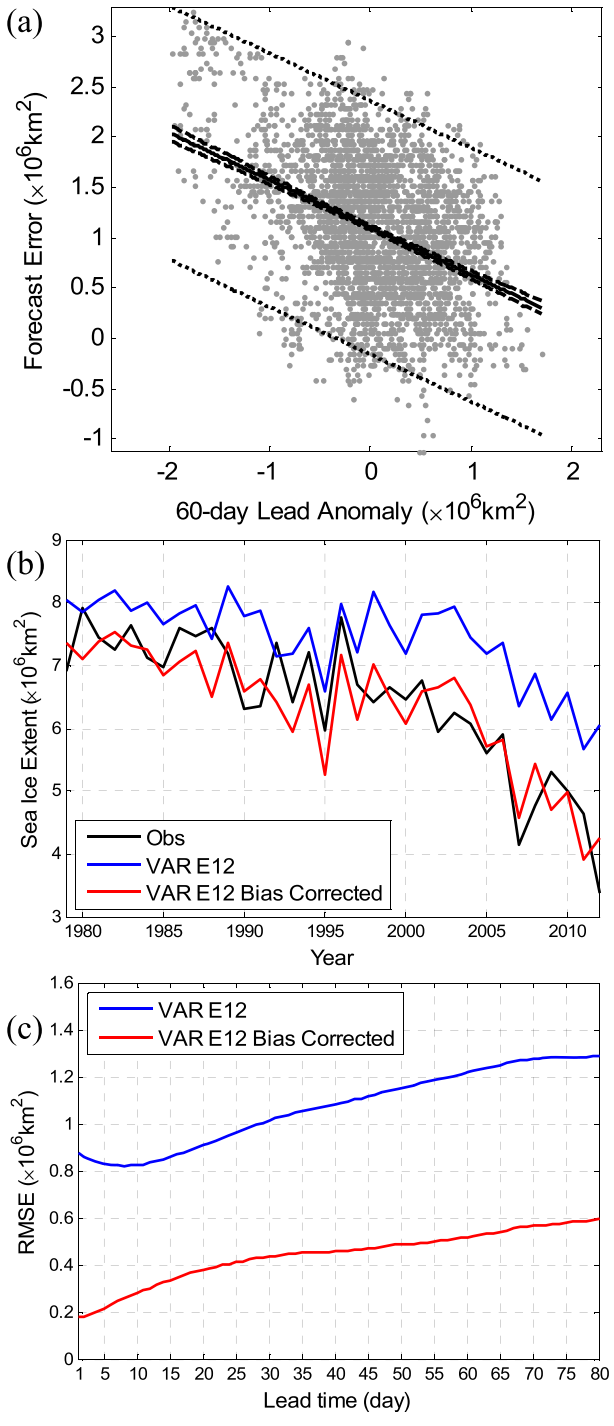

FIG. 10. (a) Scatterplot of the 60-day lead forecast error and anomaly in the SIE. The solid line represents the linear fit of the data, and the dashed (dotted) curves show the 95% confidence interval of the fit (predicted bias). (b) The 60-day lead forecast of the September SIE without (blue) and with (red) bias correction by the VAR E12 model, compared with observations (black). (c) As in (b), but for the RMSE at various lead times.

daily SIC at lead times of ~20–60 days compared with the anomaly persistence and damped anomaly persistence, as measured by the temporal anomaly correlation and root-mean-square error. The daily forecast also leads to ice-free date prediction and September mean sea ice extent prediction. The improvements over the anomaly persistence in the forecast skill are most marked at the Barents and Kara Seas, a key region for the Northeast Passage (e.g., Farré et al. 2014) and the long-range winter outlooks (e.g., Scaife et al. 2014). The September SIE minimum is also well captured by the VAR model, with the assistance of a bias-correction procedure. While the detailed mechanism leading to the high predictability of intraseasonal sea ice concentration needs to be further examined, the study reveals for the first time that Arctic sea ice concentration can be predicted statistically with reasonable skill on the intraseasonal time scales, even without direct information of the atmosphere and ocean. The intraseasonal forecast by this model is able to help bridge the gap between the short-term prediction and seasonal forecast of the Arctic sea ice conditions, a necessary step toward a seamless prediction system of the northern extratropics (e.g., Balmaseda et al. 2010; Tietsche et al. 2014).

As the atmospheric circulation can modulate the intraseasonal sea ice variability (e.g., Zhang et al. 2013), it is worthwhile to add the atmospheric variables, such as surface winds, pressure, air temperature, and cloud information, in the VAR model in the future to further improve the forecast skill, especially in the short range. In addition, the error in ice-free dates is rather large for a useful prediction product. It is thus an important challenge to explore further factors that lead to large errors and the possible improvements. Moreover, the optimal VAR model for pan-Arctic predictions, VAR E25, may not provide the best skill for regional sea ice predictions, as revealed in the examples of the Barents and Kara Seas (VAR E29 and E12, respectively; Fig. 4). This regional dependence indicates the underlying physical and dynamical differences in the local ice melting processes, which may be better addressed in regional sea ice forecast models similar to Matthewman and Magnusdottir (2011).

The same satellite SIC data have also been parallelly processed with a different algorithm developed by Cavalieri et al. (1996), commonly known as the "NASA team" SIC data (to be distinguished from the "bootstrap" data used above). These two datasets are generally in good agreement but have nonnegligible differences in many aspects (e.g., Belchansky and Douglas 2002). The VAR model has been applied to these NASA team SIC data and has achieved similar forecast skill in general with minor regional differences (not shown), indicating the forecast skill shown in this study is fairly robust to observational uncertainties.

Acknowledgments. This study was supported by the Office of Naval Research under Grant N00014-12-1-0911. The authors thank David Chapman, Dong Eun Lee, Naomi Henderson, Alexey Kaplan, Michael Ghil, Dmitri Kondrashov, and Mickaël D. Chekroun for developing an earlier version of the statistical model used in this study and for the helpful discussions, as well as three anonymous reviewers for their valuable comments.

REFERENCES

Balmaseda, M. A., L. Ferranti, F. Molteni, and T. N. Palmer, 2010: Impact of 2007 and 2008 Arctic ice anomalies on the atmospheric circulation: Implications for long-range predictions. *Quart. J. Roy. Meteor. Soc.*, **136**, 1655–1664, doi:10.1002/qj.661.

Belchansky, G. I., and D. C. Douglas, 2002: Seasonal comparisons of sea ice concentration estimates derived from SSM/I, OKEAN, and RADARSAT data. *Remote Sens. Environ.*, **81**, 67–81, doi:10.1016/S0034-4257(01)00333-9.

Cavalieri, D. J., C. L. Parkinson, P. Gloersen, and H. J. Zwally, 1996: Sea ice concentrations from *Nimbus-7* SMMR and DMSP SSM/I-SSMIS passive microwave data, version 1. NASA National Snow and Ice Data Center Distributed Active Archive Center, subset used: Northern Hemisphere daily data (updated yearly), accessed 13 May 2015, doi:10.5067/8GQ8LZQVL0VL.

Chapman, D., M. A. Cane, N. Henderson, D. E. Lee, and C. Chen, 2015: A vector autoregressive ENSO prediction model. *J. Climate*, **28**, 8511–8520, doi:10.1175/JCLI-D-15-0306.1.

Chen, D., and X. Yuan, 2004: A Markov model for seasonal forecast of Antarctic sea ice. *J. Climate*, **17**, 3156–3168, doi:10.1175/1520-0442(2004)017<3156:AMMFSF>2.0.CO;2.

Chevallier, M., D. Salas y Melia, A. Voldoire, M. Déqué, and G. Garric, 2013: Seasonal forecasts of the pan-Arctic sea ice extent using a GCM-based seasonal prediction system. *J. Climate*, **26**, 6092–6104, doi:10.1175/JCLI-D-12-00612.1.

Comiso, J. C., 2000: Bootstrap sea ice concentrations from *Nimbus-7* SMMR and DMSP SSM/I-SSMIS, version 2. National Snow and Ice Data Center Distributed Active Archive Center, subset used: Northern Hemisphere daily data (updated yearly), accessed 27 August 2014, doi:10.5067/J6JQLS9EJ5HU.

Deser, C., and H. Teng, 2008: Evolution of Arctic sea ice concentration trends and the role of atmospheric circulation forcing, 1979–2007. *Geophys. Res. Lett.*, **35**, L02504, doi:10.1029/2007GL032023.

——, J. E. Walsh, and M. S. Timlin, 2000: Arctic sea ice variability in the context of recent atmospheric circulation trends. *J. Climate*, **13**, 617–633, doi:10.1175/1520-0442(2000)013<0617:ASIVIT>2.0.CO;2.

Eicken, H., 2013: Arctic sea ice needs better forecasts. *Nature*, **497**, 431–433, doi:10.1038/497431a.

Fang, Z., and J. M. Wallace, 1994: Arctic sea ice variability on a timescale of weeks and its relation to atmospheric forcing. *J. Climate*, **7**, 1897–1914, doi:10.1175/1520-0442(1994)007<1897:ASIVOA>2.0.CO;2.

Farré, A. B., and Coauthors, 2014: Commercial Arctic shipping through the Northeast Passage: Routes, resources, governance, technology, and infrastructure. *Polar Geogr.*, **37**, 298–324, doi:10.1080/1088937X.2014.965769.

Fučkar, N. S., D. Volpi, V. Guemas, and F. J. Doblas-Reyes, 2014: A posteriori adjustment of near-term climate predictions: Accounting for the drift dependence on the initial conditions. *Geophys. Res. Lett.*, **41**, 5200–5207, doi:10.1002/2014GL060815.

Griffies, S. M., and K. Bryan, 1997: A predictability study of simulated North Atlantic multidecadal variability. *Climate Dyn.*, **13**, 459–487, doi:10.1007/s003820050177.

Guemas, V., and Coauthors, 2016: A review on Arctic sea-ice predictability and prediction on seasonal to decadal time-scales. *Quart. J. Roy. Meteor. Soc.*, doi:10.1002/qj.2401, in press.

Henderson, G. R., B. S. Barrett, and D. M. Lafleur, 2014: Arctic sea ice and the Madden–Julian oscillation (MJO). *Climate Dyn.*, **43**, 2185–2196, doi:10.1007/s00382-013-2043-y.

Holland, M. M., and C. M. Bitz, 2003: Polar amplification of climate change in coupled models. *Climate Dyn.*, **21**, 221–232, doi:10.1007/s00382-003-0332-6.

Johnstone, I., 2001: On the distribution of the largest eigenvalue in principal components analysis. *Ann. Stat.*, **29**, 295–327, doi:10.1214/aos/1009210544.

Kapsch, M.-L., R. G. Graversen, and M. Tjernström, 2013: Springtime atmospheric energy transport and the control of Arctic summer sea-ice extent. *Nat. Climate Change*, **3**, 744–748, doi:10.1038/nclimate1884.

Kharin, V. V., G. J. Boer, W. J. Merryfield, J. F. Scinocca, and W.-S. Lee, 2012: Statistical adjustment of decadal predictions in a changing climate. *Geophys. Res. Lett.*, **39**, L19705, doi:10.1029/2012GL052647.

Kim, B.-M., S.-W. Son, S.-K. Min, J.-H. Jeong, S.-J. Kim, X. Dong, T. Shim, and J.-H. Yoon, 2014: Weakening of the stratospheric polar vortex by Arctic sea-ice loss. *Nat. Commun.*, **5**, 4646, doi:10.1038/ncomms5646.

Koenigk, T., and U. Mikolajewicz, 2009: Seasonal to interannual climate predictability in mid and high northern latitudes in a global coupled model. *Climate Dyn.*, **32**, 783–798, doi:10.1007/s00382-008-0419-1.

Kravtsov, S., D. Kondrachov, and M. Ghil, 2009: Empirical model reduction and the modeling hierarchy in climate dynamics. *Stochastic Physics and Climate Modeling*, T. Palmer and T. Williams, Eds., Cambridge University Press, 35–72.

Lee, D. E., D. Chapman, N. Henderson, C. Chen, and M. Cane, 2015: Multilevel vector autoregressive prediction of sea surface temperature in the north tropical Atlantic Ocean and the Caribbean Sea. *Climate Dyn.*, 1–12, doi:10.1007/s00382-015-2825-5.

Lindsay, R. W., J. Zhang, A. J. Schweiger, and M. A. Steele, 2008: Seasonal predictions of ice extent in the Arctic Ocean. *J. Geophys. Res.*, **113**, C02023, doi:10.1029/2007JC004259.

Liu, J., J. A. Curry, H. Wang, M. Song, and R. M. Horton, 2012: Impact of declining Arctic sea ice on winter snowfall. *Proc. Natl. Acad. Sci. USA*, **109**, 4074–4079, doi:10.1073/pnas.1114910109.

Liu, Z., and M. Alexander, 2007: Atmospheric bridge, oceanic tunnel, and global climatic teleconnections. *Rev. Geophys.*, **45**, doi:10.1029/2005RG000172.

Love, B. S., A. J. Matthews, and G. J. Janacek, 2008: Real-time extraction of the Madden–Julian oscillation using empirical mode decomposition and statistical forecasting with a VARMA model. *J. Climate*, **21**, 5318–5335, doi:10.1175/2008JCLI1977.1.

Lütkepohl, H., 2005: *New Introduction to Multiple Time Series Analysis.* Springer, 764 pp.

Matthewman, N. J., and G. Magnusdottir, 2011: Observed interaction between Pacific sea ice and the western Pacific pattern on intraseasonal time scales. *J. Climate*, **24**, 5031–5042, doi:10.1175/2011JCLI4216.1.

Merryfield, W. J., W. S. Lee, W. Wang, M. Chen, and A. Kumar, 2013: Multi-system seasonal predictions of Arctic sea ice. *Geophys. Res. Lett.*, **40**, 1551–1556, doi:10.1002/grl.50317.

Msadek, R., G. A. Vecchi, M. Winton, and R. G. Gudgel, 2014: Importance of initial conditions in seasonal predictions of Arctic sea ice extent. *Geophys. Res. Lett.*, **41**, 5208–5215, doi:10.1002/2014GL060799.

Parkinson, C. L., and D. J. Cavalieri, 2008: Arctic sea ice variability and trends, 1979–2006. *J. Geophys. Res.*, **113**, C07003, doi:10.1029/2007JC004558.

Peterson, K. A., A. Arribas, H. T. Hewitt, A. B. Keen, D. J. Lea, and A. J. McLaren, 2015: Assessing the forecast skill of Arctic sea ice extent in the GloSea4 seasonal prediction system. *Climate Dyn.*, **44**, 147–162, doi:10.1007/s00382-014-2190-9.

Polyakov, I. V., A. V. Pnyushkov, and L. A. Timokhov, 2012: Warming of the intermediate Atlantic water of the Arctic Ocean in the 2000s. *J. Climate*, **25**, 8362–8370, doi:10.1175/JCLI-D-12-00266.1.

Porter, D. F., J. J. Cassano, and M. C. Serreze, 2012: Local and large-scale atmospheric responses to reduced Arctic sea ice and ocean warming in the WRF Model. *J. Geophys. Res.*, **117**, D11115, doi:10.1029/2011JD016969.

Scaife, A. A., and Coauthors, 2014: Skillful long-range prediction of European and North American winters. *Geophys. Res. Lett.*, **41**, 2514–2519, doi:10.1002/2014GL059637.

Screen, J. A., C. Deser, I. Simmonds, and R. Tomas, 2013: Atmospheric impacts of Arctic sea-ice loss, 1979–2009: Separating forced change from atmospheric internal variability. *Climate Dyn.*, **43**, 333–344, doi:10.1007/s00382-013-1830-9.

Seierstad, I. A., and J. Bader, 2009: Impact of a projected future Arctic sea ice reduction on extratropical storminess and the NAO. *Climate Dyn.*, **33**, 33 937–33 943, doi:10.1007/s00382-008-0463-x.

Serreze, M. C., and Coauthors, 2003: A record minimum Arctic sea ice extent and area in 2002. *Geophys. Res. Lett.*, **30**, 1110, doi:10.1029/2002GL016406.

——, M. M. Holland, and J. Stroeve, 2007: Perspectives on the Arctic's shrinking sea-ice cover. *Science*, **315**, 1533–1536, doi:10.1126/science.1139426.

Sigmond, M., J. C. Fyfe, G. M. Flato, V. V. Kharin, and W. J. Merryfield, 2013: Seasonal forecast skill of Arctic sea ice area in a dynamical forecast system. *Geophys. Res. Lett.*, **40**, 529–534, doi:10.1002/grl.50129.

Simmonds, I., 2015: Comparing and contrasting the behavior of Arctic and Antarctic sea ice over the 35 year period 1979–2013. *Ann. Glaciol.*, **56**, 18–28, doi:10.3189/2015AoG69A909.

Smedsrud, L. H., and Coauthors, 2013: The role of the Barents Sea in the Arctic climate system. *Rev. Geophys.*, **51**, 415–449, doi:10.1002/rog.20017.

Stammerjohn, S. E., D. G. Martinson, R. C. Smith, X. Yuan, and D. Rind, 2008: Trends in Antarctic annual sea ice retreat and advance and their relation to El Niño–Southern Oscillation and southern annular mode variability. *J. Geophys. Res.*, **113**, C03S90, doi:10.1029/2007JC004269.

——, R. Massom, D. Rind, and D. Martinson, 2012: Regions of rapid sea ice change: An inter-hemispheric seasonal comparison. *Geophys. Res. Lett.*, **39**, L06501, doi:10.1029/2012GL050874.

Stroeve, J., L. C. Hamilton, C. M. Bitz, and E. Blanchard-Wrigglesworth, 2014: Predicting September sea ice: Ensemble skill of the SEARCH Sea Ice Outlook 2008–2013. *Geophys. Res. Lett.*, **41**, 2411–2418, doi:10.1002/2014GL059388.

Strong, C., G. Magnusdottir, and H. Stern, 2009: Observed feedback between winter sea ice and the North Atlantic Oscillation. *J. Climate*, **22**, 6021–6032, doi:10.1175/2009JCLI3100.1.

Tietsche, S., and Coauthors, 2014: Seasonal to interannual Arctic sea ice predictability in current global climate models. *Geophys. Res. Lett.*, **41**, 1035–1043, doi:10.1002/2013GL058755.

Wallace, J. M., and D. S. Gutzler, 1981: Teleconnections in the geopotential height field during the Northern Hemisphere winter. *Mon. Wea. Rev.*, **109**, 784–812, doi:10.1175/1520-0493(1981)109<0784:TITGHF>2.0.CO;2.

Wang, L., M. Ting, D. Chapman, D. E. Lee, N. Henderson, and X. Yuan, 2015: Prediction of northern summer low-frequency circulation using a high-order vector auto-regressive model. *Climate Dyn.*, 1–17, doi:10.1007/s00382-015-2607-0.

Wang, W., M. Chen, and A. Kumar, 2013: Seasonal prediction of Arctic sea ice extent from a coupled dynamical forecast system. *Mon. Wea. Rev.*, **141**, 1375–1394, doi:10.1175/MWR-D-12-00057.1.

Wilks, D. S., 1995: *Statistical Methods in the Atmospheric Sciences: An Introduction*. Academic Press, 467 pp.

Yang, X.-Y., and X. Yuan, 2014: The early winter sea ice variability under the recent Arctic climate shift. *J. Climate*, **27**, 5092–5110, doi:10.1175/JCLI-D-13-00536.1.

Zhang, J., R. Lindsay, A. Schweiger, and M. Steele, 2013: The impact of an intense summer cyclone on 2012 Arctic sea ice retreat. *Geophys. Res. Lett.*, **40**, 720–726, doi:10.1002/grl.50190.